

Intermediate-Depth Earthquakes in a Region of Continental Convergence: South Island, New Zealand

by Monica D. Kohler and Donna Eberhart-Phillips

Abstract It is rare to find earthquakes with depths greater than 30 km in continent–continent collision zones because the mantle lithosphere is usually too hot to enable brittle failure. However, a handful of small, intermediate-depth earthquakes (30–97 km) have been recorded in the continental collision region in central South Island, New Zealand. The earthquakes are not associated with subduction but all lie within or on the margins of thickened crust or uppermost mantle seismic high-velocity anomalies. The largest of the earthquakes has M_L 4.0 corresponding to a rupture radius of between 100 and 800 m, providing bounds on the upper limit to the rupture length over which brittle failure is taking place in the deep brittle–plastic transition zone. The earthquake sources may be controlled by large shear strain gradients associated with viscous deformation processes in addition to depressed geotherms.

Introduction

The majority of earthquakes involve sudden brittle failure on preexisting planes of weakness during which the frictional sliding causes elastic waves to radiate (Scholz, 1990). For most intermediate-depth earthquakes (depths between 30 and 100 km), subduction zones provide the relatively cool, brittle environment in which the displacement takes place. However, small, infrequent mantle earthquakes occur below the continental collision zone in South Island, New Zealand, that is associated with viscously deforming, thickening lithosphere rather than subduction. Earthquakes with hypocentral depths greater than 30 km in continental settings are usually attributed to cooler-than-average environments in which geotherms are depressed (Chen and Molnar, 1983; Allis and Shi, 1995). The spatial patterns in the South Island, New Zealand, mantle earthquake hypocenters relative to regional tomographic P -wave velocity images (Kohler and Eberhart-Phillips, 2002) illustrate that lower-than-average uppermost mantle temperatures alone do not explain their occurrence. The earthquake data provide an unusual glimpse into the rheological environment of the brittle–plastic transition zone.

The central segment of the north-northeast–south-southwest trending Alpine fault bounds Pacific plate rocks to the east, which are moving south and also overthrusting Australian plate rocks, resulting in the uplift of the Southern Alps during the past 5–7 m.y. (Wellman, 1953; Walcott, 1978; Norris *et al.*, 1990) (Fig. 1). The Pacific and Australian plates are converging obliquely in South Island, and lithospheric thickening is taking place to accommodate the shortening (Walcott, 1998). The Southern Alps in South Island, New Zealand, are the product of the early stages of oblique con-

tinental collision between the Pacific and Australian plates. The convergence in northern South Island is accommodated by a broad region of faulting in the overlying Australian plate and northwest subduction of the Pacific plate at the Hikurangi Trench. By contrast, in southwestern South Island, the Australian plate is oceanic and is subducting eastward below the Pacific plate at the Puysegur Trench and Fiordland Trough.

The Alpine fault crosses most of South Island and accommodates 50%–70% of total plate displacement (Beavan *et al.*, 1999; Norris and Cooper, 2000; Sutherland *et al.*, 2000). The plate boundary crosses South Island continental crust as a broad zone of distributed deformation. Seismicity is distributed in a region 100–300 km wide, mostly east of the Alpine fault (Walcott, 1978; Leitner *et al.*, 2001). Unlike the Hikurangi and Puysegur subduction regions, there is very little seismicity below 30 km in the Southern Alps (Fig. 2). Crustal thickness varies from 30–45 km across the Southern Alps (Woodward, 1979; Allis, 1986; Smith *et al.*, 1995; Wilson and Eberhart-Phillips, 1998). The crust is thickest 10 km east of the highest topography and south of the highest peaks at the southern end of the Southern Alps (Reilly and Whiteford, 1979; Norris *et al.*, 1990; Davey *et al.*, 1998). Southern Alps uplift began ~7 m.y.a. in the southern end and ~5 m.y.a. in the northern end leading to lateral temperature variations in the lower crust and upper mantle (Allis and Shi, 1995). Intermediate-depth seismicity in central South Island is clustered near the southern end of the Southern Alps (Fig. 2), where significantly more crustal thickening has occurred than in the northern end (Eberhart-Phillips and Reyners, 1997, 2001; Eberhart-Phillips and Bannister, 2002).

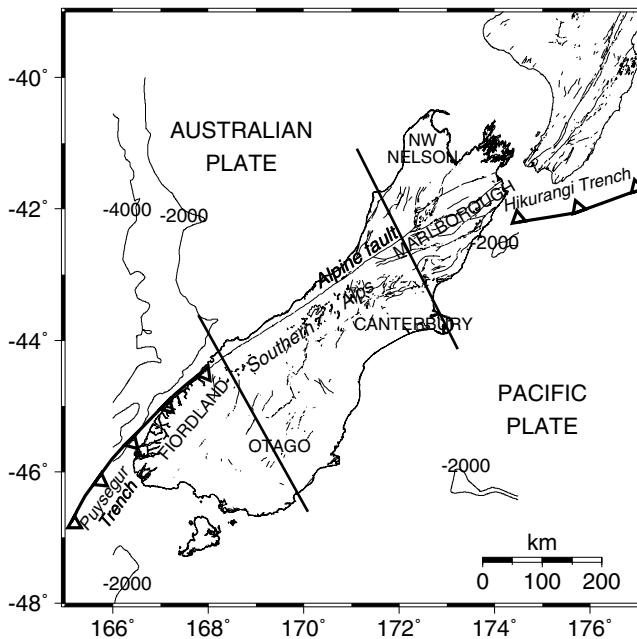


Figure 1. South Island, New Zealand, plate tectonic setting showing active fault systems. The Hikurangi and Puysegur subduction zones are indicated by curves with triangular tick marks showing the direction of subduction. The region lying between the two black lines includes the transpressional plate boundary system whose deformation involves Alpine fault-parallel shear as well as fault-perpendicular continental collision. Bathymetry contours corresponding to -2000 m and -4000 m are also shown.

Data and Hypocenter Relocation Approach

The New Zealand National Seismograph Network (NZNSN) has been systematically recording earthquakes throughout South Island since the 1960s as described by Reyners (1989). Prior to 1990, stations recorded onto velocorders, and the station spacing on South Island was 100–250 km. The epicentral patterns were reliable, but the depths were poorly constrained in central South Island; hence, depths of earthquakes outside the subduction zones were fixed to 12 or 33 km. An opportunity for accurate depth determination for Southern Alps earthquakes came with the Pukaki microearthquake network, which operated from 1975–1983 to monitor reservoir-induced seismicity (Haines *et al.*, 1979; Reyners 1988). The spatially small, dense network also had a lower magnitude threshold than the NZNSN, being complete for $M_L \geq 1.8$. It recorded 2825 earthquakes of which only a few were deep. Reyners (1987) analyzed the 23 Pukaki earthquakes deeper than 25 km and inferred a shallowly northwest-dipping subcrustal seismic zone to a depth of 70 km.

Imaging the Southern Alps and the Alpine fault was the focus of multinational active and passive seismic experiments conducted from 1995 to 1997 (Stern *et al.*, 1997). Eberhart-Phillips and Bannister (2002) used those data to-

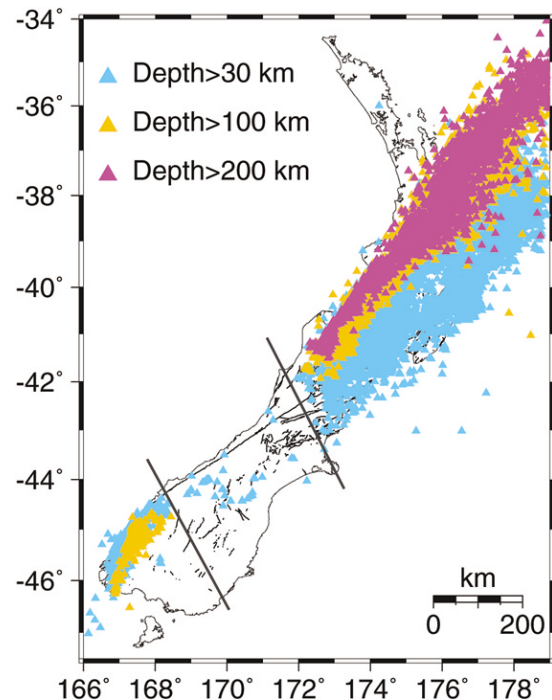


Figure 2. South Island, New Zealand, intermediate-depth and deep seismicity from the 1990–2000 NZNSN catalog, which is complete for $M_L \geq 3.0$. Black lines are the same as in Figure 1.

gether with the deep Pukaki network earthquakes to obtain a three-dimensional velocity model in the Southern Alps region. Their simultaneous inversion for hypocenters and velocity provides more accurate hypocenters than Reyners' (1987) one-dimensional model and allows for the joint interpretation of seismicity and velocity features. The three-dimensional velocity model was also used to account for crustal heterogeneity in the regional uppermost mantle model based on teleseismic travel-time data (Kohler and Eberhart-Phillips, 2002).

We investigated additional deep crustal and subcrustal earthquakes outside the limited region and time period covered by the Pukaki network by analyzing NZNSN data. The NZNSN was upgraded from 1987–1990 with improved instrumentation to produce digital waveform data. Additional stations reduced the station spacing to ~ 100 km. Since 1990, the network has been composed of short-period stations that record high-quality waveform data with uniform digitization and timing methods.

We obtained NZNSN data from 1990–2000 for all Southern Alps region earthquakes with catalog depths greater than 20 km. Examination of waveforms showed that NZNSN analysts' picks that resulted in the catalog hypocenters were good. The earthquakes were relocated using P and S data with the Southern Alps three-dimensional velocity model (Eberhart-Phillips and Bannister, 2001). Sixteen earthquakes had hypocentral depths ≥ 30 km (Table 1).

The depth uncertainty computed from the covariance

Table 1
Central South Island Earthquakes with Depths ≥ 30 km*

Date	Time (UTC)	Latitude	Longitude	Depth (km)	M_L	Number of Observations	Depth Uncertainty (km)	Seismic Network
March 26, 1990	22:31:15.27	43S55.87	169E00.60	75	3.0	13	± 5	NZNSN
May 2, 1990	13:51:08.63	43S30.32	169E55.34	64	3.6	14	± 5	NZNSN
June 26, 1990	18:40:14.18	44S18.09	168E53.26	35	4.0	18	± 5	NZNSN
March 10, 1992	22:19:12.47	42S36.48	171E08.92	97	3.4	16	± 5	NZNSN
January 25, 1993	10:32:46.05	44S16.96	169E10.19	39	3.1	14	± 5	NZNSN
August 20, 1993	00:29:36.52	44S23.11	170E34.50	43	3.2	15	± 5	NZNSN
April 15, 1996	00:04:01.73	44S21.00	170E38.27	30	3.1	18	± 5	NZNSN
July 5, 1996	04:10:51.60	44S03.46	169E19.50	43	3.1	8	± 5	NZNSN
February 20, 1997	09:15:53.45	42S47.82	171E17.70	69	3.5	15	± 5	NZNSN
September 26, 1999	12:15:41.84	44S00.03	169E29.48	49	3.2	18	± 5	NZNSN
October 10, 1999	17:20:42.29	44S11.97	169E00.15	66	3.2	22	± 5	NZNSN
December 27, 1990	17:26:10.51	43S34.42	171E52.15	70	3.1	11	± 15	NZNSN
December 27, 1990	17:29:12.18	43S34.38	171E47.76	51	3.0	12	± 15	NZNSN
September 26, 1991	16:36:36.41	44S00.36	169E31.13	38	3.2	16	± 15	NZNSN
November 30, 1993	20:49:53.46	44S01.57	172E13.29	41	3.1	9	± 15	NZNSN
May 14, 1995	19:49:30.36	44S14.42	168E58.55	52	3.7	18	± 15	NZNSN
February 16, 1976	07:41:49.04	44S25.92	170E 6.12	32	2.4	12	± 5	Pukaki
March 17, 1976	13:27:06.28	43S59.72	169E26.61	64	3.8	13	± 5	Pukaki
August 5, 1976	17:18:30.17	43S49.13	169E53.54	60	3.3	12	± 5	Pukaki
July 28, 1977	20:22:49.79	44S02.85	169E21.67	61	3.6	13	± 5	Pukaki
October 12, 1978	01:40:02.93	44S25.77	170E26.07	35	2.7	10	± 5	Pukaki
March 1, 1979	11:48:39.38	44S15.90	170E42.49	31	1.9	6	± 5	Pukaki
March 12, 1979	08:02:33.20	44S02.06	169E25.61	64	3.5	12	± 5	Pukaki
October 24, 1979	22:18:39.25	43S58.42	170E47.07	31	2.1	7	± 5	Pukaki
January 9, 1980	01:26:16.94	44S25.34	170E25.67	34	3.1	12	± 5	Pukaki
May 4, 1980	21:02:21.10	44S32.05	169E54.07	48	3.5	12	± 5	Pukaki
July 20, 1980	07:41:18.38	44S20.74	169E39.87	42	3.3	11	± 5	Pukaki
July 30, 1981	07:34:29.46	44S03.24	169E43.04	52	2.6	8	± 5	Pukaki
August 3, 1981	18:04:36.96	44S18.98	170E42.78	30	2.1	8	± 5	Pukaki
August 23, 1981	02:15:56.09	44S18.66	170E29.58	30	1.8	13	± 5	Pukaki
February 18, 1982	02:28:50.44	44S19.24	169E56.58	45	2.4	11	± 5	Pukaki
June 16, 1982	02:28:17.42	43S59.25	170E44.83	44	3.0	11	± 5	Pukaki
January 27, 1983	22:18:33.82	44S11.74	169E52.42	44	2.8	14	± 5	Pukaki
January 29, 1983	21:08:13.51	44S11.91	169E53.17	42	2.7	18	± 5	Pukaki
October 29, 1983	19:16:36.63	43S56.81	170E59.30	43	2.5	14	± 5	Pukaki

*Recorded by the New Zealand National Seismograph Network between 1990 and 1998 and by the Pukaki network (Reyners, 1987).

ranged from 0.6 to 5.3 km for the NZNSN events and from 0.5 to 2.6 km for the Pukaki events. To evaluate how well constrained the depths were, we ran the location inversions with varied S weighting, varied initial depths, and varied distance weighting. For most of the earthquakes, the depths were robust with the differing location factors resulting in consistent depths of within 5 km. Some earthquakes had hypocentral depths that were consistently deep (>33 km), but they were poorly constrained and varied by up to 15 km with differing location factors. Gomberg *et al.* (1990) estimated that S arrivals from stations within a distance equivalent to 1.4 focal depths are needed to get reliable hypocentral depths, accurate to 1.5 km in their study. By this criteria, the Pukaki earthquake depths are excellent since they all have stations within one focal depth. All but three of the NZNSN earthquakes have stations within 1.4 focal depths.

While the NZNSN is sparse, the 100-km station spacing is generally adequate to obtain reliable depths for subcrustal

earthquakes. The 20 February 1997 earthquake is shown for example in Figure 3. The seismograms for the four closest three-component stations are shown in azimuthal order. The P and S arrivals can be picked and the data cannot be fit except by a deep hypocenter. The depth is 69 km and the distance to the closest station is 55 km. Thus, this is clearly a deep earthquake, despite being the only deep earthquake recorded in that vicinity.

The 1990–2000 NZNSN catalog is complete for $M_L \geq 3.0$ and contains few earthquakes with magnitudes smaller than this (Anderson and Webb, 1994). The maximum magnitude for all central South Island intermediate-depth earthquakes recorded in 11 yr is M_L 4.0. If a larger, intermediate-depth earthquake had occurred during the 11 yr of data recording, the network would have recorded it. None of the earthquakes is large enough or has enough three-component recordings within 75 km of the epicenter to obtain a focal mechanism (e.g., Robinson and Webb, 1996). However,

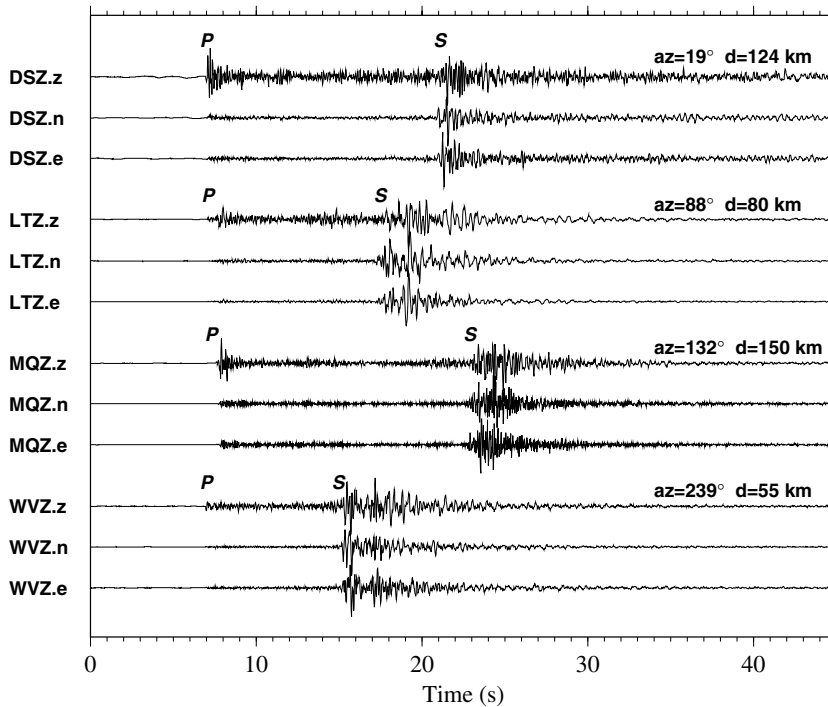


Figure 3. Seismograms for the 20 February 1997 earthquake (69-km depth) showing *P* and *S* waves. Station components are indicated to the left of waveform, and azimuth (“az”) and distance from earthquake (“d”) are indicated on the right.

Reyners (1987) concluded that the composite first motion data for the Pukaki network mantle earthquakes were consistent with a *P* axis for subhorizontal compression in the direction of plate convergence.

Discussion

When the epicenters of the mantle earthquakes are plotted on top of regional tomographic images of *P*-wave velocity variations (Kohler and Eberhart-Phillips, 2002), they are found to lie either within or on the margins of an uppermost mantle high-velocity anomaly (Fig. 4). The three-dimensional tomographic images were obtained by teleseismic *P*-wave travel-time residual inversion. The inversion data consisted of teleseismic travel times measured from the NZNSN waveforms and from waveforms recorded during the 1995–1996 Southern Alps Passive Seismic Experiment (Anderson *et al.*, 1997). Crustal heterogeneity was accounted for by ray tracing through an independently obtained three-dimensional crustal velocity and Moho depth model (Eberhart-Phillips and Reyners, 1997, 2001; Eberhart-Phillips and Bannister, 2002). The images show a near-vertical, high-velocity (2%–4%) structure in the uppermost mantle that underlies thickened crust along the north-northeast–south-southwest axis of the Southern Alps. The center of the high-velocity anomaly lies to the east of the Alpine fault and below thickened crust.

The mass flow along strike presents problems in quantitatively applying two-dimensional dynamic models to understand the deformation environment, but commonalities among them provide qualitative insights. The Southern Alps uppermost mantle high-velocity anomalies have been ex-

plained by lithospheric thickening below the center of convergence by means of a vertical downwelling (Stern *et al.*, 2000; Pysklywec *et al.*, 2002), although lateral shear strain is also a significant component of plate motion. Kinematic lithospheric deformation simulations predict crustal thickening due to plate bending and crustal flow parallel to the axis of thickening along an axis 10°–15° counterclockwise from the plate boundary shear zone (Gerbault *et al.*, 2002). At the base of the crust, the maximum shear stress is at the zone of thickening. At greater depths in the lithosphere, the regions of maximum shear stress underlie the Alpine fault and the eastern edge of the Southern Alps with stresses in the downwelling region comparable to those in a bending layer. Gravitational instability can thicken the lithosphere and result in a deep, high-density body (Houseman *et al.*, 2000). Depending on the rheology, the distributed thickening may exhibit subduction-like behavior in the uppermost mantle (Beaumont *et al.*, 1996). One commonality among the models discussed above is that they predict a horizontal shear zone with high strain rate in the lithospheric mantle on the northwest side of the high-velocity body, broadly underlying the Alpine fault and coinciding with the mantle earthquake locations.

If temperature in the form of depressed geotherms were the sole factor controlling the location of intermediate-depth earthquakes, then the earthquakes should all occur within the fastest and presumably most downwarped portion of the lithosphere. Indeed the shallowest intermediate-depth earthquakes are found to lie below or near the deepest part of the crustal root (Fig. 5). If we assume that tectonic convergence has thickened the uppermost mantle lithosphere by at least 20 km (corresponding to similarly thickened crust overhead)

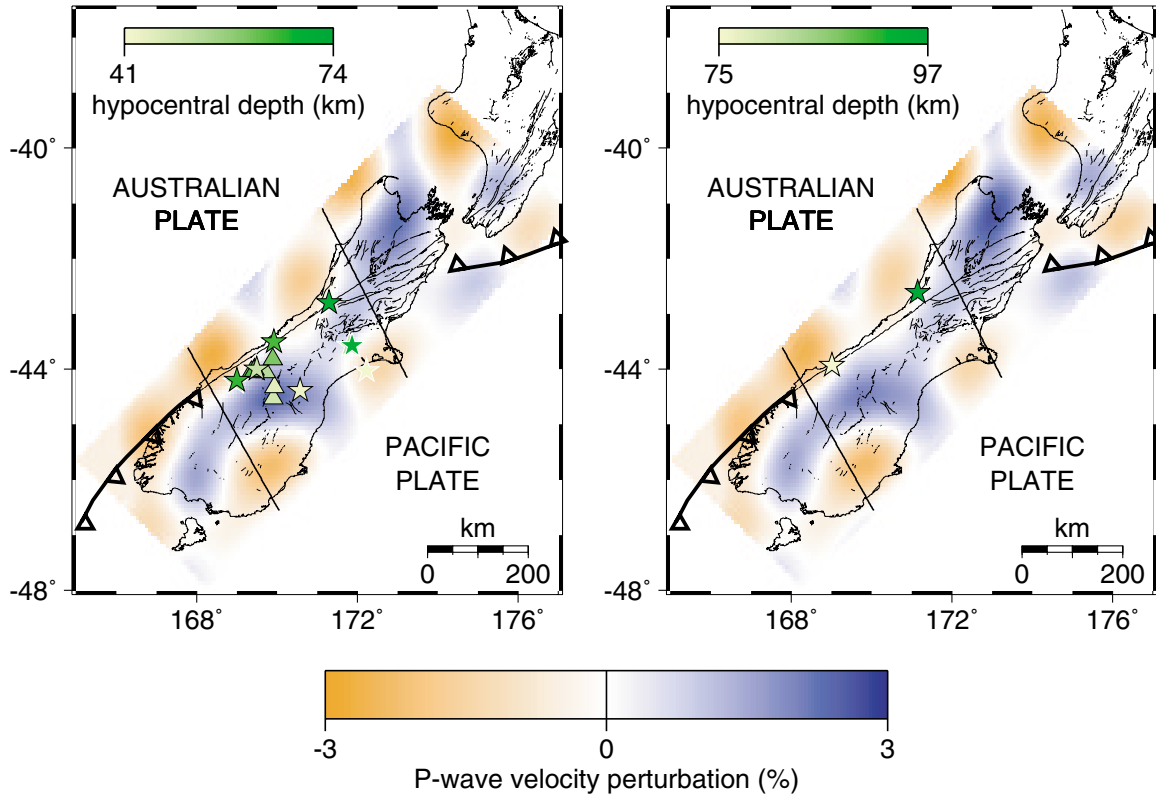


Figure 4. Upper mantle P -wave velocity variations for depths of 60 km (left) and 85 km (right) determined from an independent study of mantle lithospheric seismic structure from teleseismic travel-time residual inversion (Kohler and Eberhart-Phillips, 2002). Relocated central South Island upper mantle earthquake epicenters (Table 1) corresponding to each velocity variation depth slice are shown in each plot. Pukaki network (Reyners, 1987) relocated epicenters are shown by triangles and NZNSN relocated epicenters by stars. Black outlines on symbols indicate a hypocentral depth uncertainty of ± 5 km; white outlines indicate an uncertainty of ± 15 km. Green color scales at top left indicate hypocentral depth ranges and orange–blue color scale at bottom indicates P -wave velocity perturbation range. Black lines are the same as in Figure 1.

and that initially horizontal geotherms in the shallowest uppermost mantle are approximately defined according to $\delta T/\delta z \approx 10^\circ\text{C}/\text{km}$ (Turcotte and Schubert, 1982), then the smaller, convergence-centered earthquakes occurred within material having temperatures $\sim 500^\circ\text{C}$ for rock vertically displaced from an ~ 50 -km depth. This assumes that heat is transported by conduction and that the depressed lithosphere has not had enough time to thermally equilibrate. This standard linear gradient is a conservative estimate and so provides a lower bound on the temperature of mantle below the convergent zone. (On the other hand the uppermost mantle may be considerably cooler if active downwelling is occurring.) In any case, this argument explains only the existence of seismicity near the center of the high-velocity anomaly and crustal root.

The lower crustal and shallowest upper mantle earthquakes lie within the high-velocity anomaly, but the deeper uppermost mantle earthquakes lie on the margins. Lateral seismic velocity anomalies are often associated with hetero-

geneous temperature fields within the mantle where high velocities are assumed to be the signature of colder-than-average uppermost mantle rock. The relationship between lateral velocity variations and temperature, $\delta V_p/\delta T = \alpha$, is uncertain with $\alpha \sim 5 \times 10^{-4} \text{ km/sec}/^\circ\text{C}$ (Anderson and Isaak, 1995) but since the relationship is linear, patterns in the predicted temperature variation maps are proportional to the seismic heterogeneity. Regardless of choice of α however, temperature gradients also do not explain the existence of the deeper earthquakes on the margins of the high-velocity anomaly where uppermost mantle is not expected to be much cooler than adjacent material at the same depth.

The locations of the mantle events more closely correspond to regions that may be experiencing the largest shear strain gradients associated with lithospheric viscous deformation. Large horizontal and vertical shear strains have been modeled for downwelling mantle lithosphere below converging continents within a two-dimensional slice parallel to the convergent zone (Houseman *et al.*, 2000). The largest

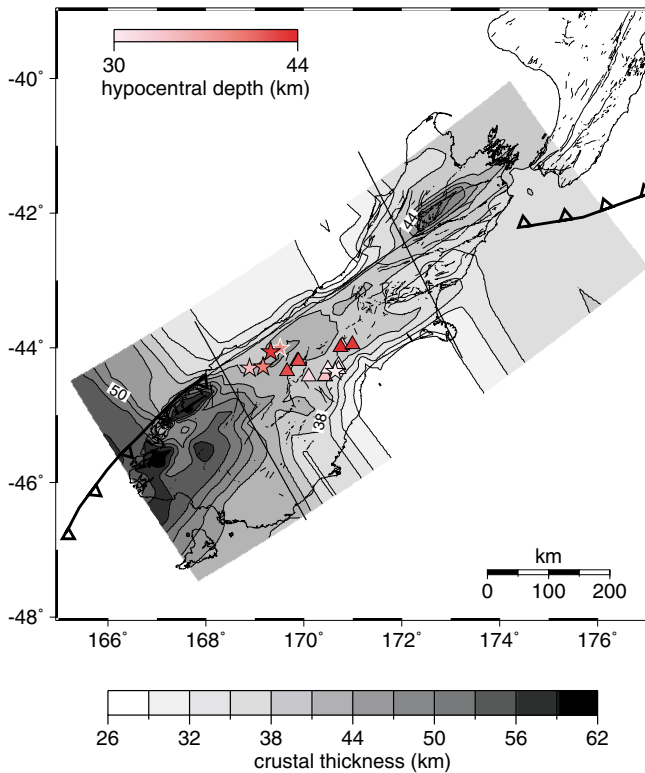


Figure 5. Crustal thickness below South Island approximated from the 7.8 km/sec isovelocity surface from local earthquake travel-time inversion (Eberhart-Phillips and Reyners, 1997, 2001; Eberhart-Phillips and Bannister, 2002) (note that the shallow high-velocity anomaly in Fiordland is not Moho variation). Central South Island crustal earthquake epicenters (Table 1) are also plotted. Pukaki network (Reyners, 1987) relocated epicenters are shown by triangles and NZNSN relocated epicenters by stars. Red color scale at top left shows variation in hypocentral depths and the gray scale at bottom shows crustal thickness variation. Black outlines on symbols indicate a hypocentral depth uncertainty of ± 5 km; white outline indicates an uncertainty of ± 15 km. Black lines are the same as in Figure 1.

shear strains are predicted to occur in the bends and in the drip of the descending mantle, and the largest strain gradients (i.e., relative displacement) occur within the axial surfaces of the bends and along the outer margins of the downwelling (Fig. 6). In addition, large dextral shear strain occurs in the lithosphere within 50 km northeast of the Alpine fault (Beavan *et al.*, 1999), which may explain why the deep earthquakes are more numerous on the northwestern side of the high-velocity body.

Using M_L 4.0 as the maximum-size recorded earthquake below 30 km in central South Island, bounds on the maximum rupture area are computed assuming shallow earthquake scaling relationships and constant stress drop (Abercrombie, 1995) (Table 2). Stress drops for M_L 4.0 lie in the range 0.5 and 50 MPa. For shallow earthquakes, there is no evidence for a stress drop dependence on depth (Mori *et al.*,

2002). The relationship between M_L and M_w for New Zealand is based on studies of larger (M_L 4.1–6.2), shallow earthquakes. The dependence lies in the range between $M_w \cong M_L - 0.25$ and $M_w \cong M_L - 0.7$ (Abercrombie *et al.*, 2001; Leitner *et al.*, 2001), both of which are used here to establish the maximum rupture radius bounds. Maximum rupture radius is found to lie between 200 and 500 m, corresponding to a maximum rupture area of between 0.2 and 0.6 km² assuming circular rupture and a constant stress drop of 3 MPa. The total range of calculations provides bounds on the upper limit to the area over which brittle failure is taking place in the deep brittle–plastic transition zone (Table 2).

The brittle–plastic transition can be a broad zone rather than occur at a single specific depth because of the polyphase nature of rock and variable strain rate (Scholz, 1990). The uppermost mantle earthquakes indicate that the transitional regime below central South Island comprises a frictional slip environment in the high shear strain gradient region of the mantle lithosphere where temperatures are still cool enough for occasional brittle or semibrittle failure to occur (Fig. 6). Patches of upper mantle rock capable of brittle failure have dimensions that are limited by surrounding plastic deformation rheology that becomes increasingly dominant with depth (Kirby, 1980). The earthquakes may be the consequence of a semibrittle faulting regime in the vertically wide brittle–plastic transition zone in which localized faults form, but their numbers and lengths are limited by high densities of dislocations near the fault tips and edges (Hirth and Tullis, 1994).

The Pacific–North American plate boundary in Southern California is also thought to consist of a high-velocity uppermost-mantle downwelling (Humphreys and Clayton, 1990; Houseman *et al.*, 2000) but no seismicity deeper than 27 km is observed (Richards-Dinger and Shearer, 2000). The regional Southern California average uppermost mantle P -wave velocity is low (≤ 7.8 km/sec) (Hadley and Kanamori, 1977; Hearn and Clayton, 1986; Richards-Dinger and Shearer, 1997) implying an environment too warm to enable deep crustal or mantle seismicity. In contrast, South Island uppermost mantle is characterized by an average P -wave velocity of 8.1–8.2 km/sec (Davey *et al.*, 1998). If South Island convergence has depressed the brittle–plastic transition zone, this supports a scenario in which the relatively deep transition zone consists of patches of mantle rock with crack lengths on the order of 1 km or less undergoing brittle failure within a matrix of plastically deforming rock. Since only small earthquakes have occurred, they cannot be observed in teleseismic data. Thus, any conclusions regarding the depth distribution of seismicity based only on teleseismically observed intermediate and large earthquakes may need to be re-evaluated (Maggi *et al.*, 2000). The Gutenberg–Richter relation that predicts greater magnitudes may be truncated at a cut-off magnitude corresponding to the maximum dimension of the brittle zone (Gutenberg and Richter, 1941, 1944). Once the brittle failure

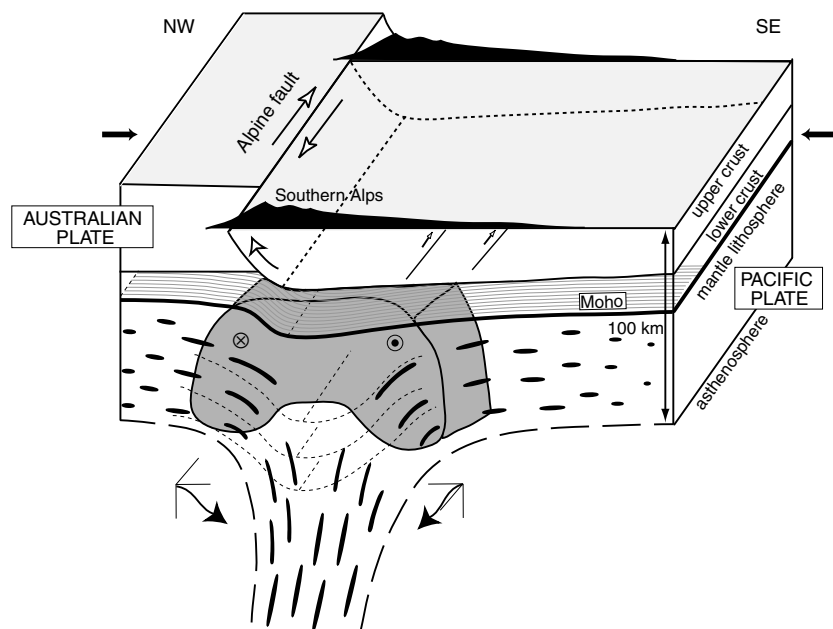


Figure 6. Schematic of deforming lithosphere and strain ellipses predicted from a qualitative compilation of the two-dimensional and three-dimensional kinematic and dynamic models (Beaumont *et al.*, 1996; Houseman *et al.*, 2000; Stern *et al.*, 2000; Gerbault *et al.*, 2002; Pysklywec *et al.*, 2002). Vertical to horizontal scale is 1:1. The largest vertical shear strain gradients occur within the axial surfaces of the bends and along the outer margins of the downwelling where relative slip between mantle lithosphere and adjacent asthenosphere most likely occurs (Houseman *et al.*, 2000). The largest horizontal shear strains occur along an axis parallel to the Alpine fault. The overlap in maximum shear strain gradient field and depressed geotherm field is shown in dark gray and represents the transition region where small patches of brittle failure may occur in the upper mantle. Large arrows with unfilled heads show direction of strike slip and reverse slip on the Alpine fault; small arrows with unfilled heads show reverse slip in the compressional region east of plate boundary. Short arrows with filled heads indicate the direction of convergence at the plate boundary. The curved arrows in the uppermost mantle plotted on top of coordinate axes represent the distributed ductile shear in three dimensions.

Table 2
Computed Upper and Lower Bounds on Rupture Radius and Area

M_w	Seismic Moment (N m)	Stress Drop (MPa)	Radius (m)	Rupture Area (km ²)
3.8	5×10^{14}	0.5	759	1.8
3.3	9×10^{13}	0.5	427	0.6
3.8	5×10^{14}	3	418	0.6
3.3	9×10^{13}	3	235	0.2
3.8	5×10^{14}	50	164	0.08
3.3	9×10^{13}	50	92	0.03

For maximum size $M_L = 4.0$ intermediate-depth earthquake recorded in central South Island.

takes place, the crack tip cannot propagate very far before plastic deformation takes over. The transition rheology determines that these deep earthquakes may always be small in magnitude and rupture dimension. When the uppermost mantle becomes hot enough with increasing depth, brittle failure no longer occurs.

Conclusions

It is highly unusual to record subcrustal earthquakes in any continental lithospheric region in such numbers with high location accuracy. Regional New Zealand seismic networks have made observations in the patterns of South Island seismicity and correlations with seismic high-velocity mapping possible. Hypocentral relocation with three-dimen-

sional velocity models confirms that the earthquakes occur in the continental mantle, and depressed geotherm calculations argue that relatively low temperatures alone cannot be responsible for the mantle earthquakes. The strong correlation between hypocenter pattern and mantle seismic anomalies suggests that the shear strain field may also be controlling their occurrence. Theoretical kinematic and dynamic simulations of the transpressional plate boundary deformation provide strong evidence for dependence on the shear strain field. The mantle earthquakes are all small, and their magnitudes illustrate that rupture takes place on patches of 2 km² or less within mantle rock that is deforming primarily by viscous flow processes.

Acknowledgments

This work was supported by NSF Grant EAR-9805224 and the New Zealand Foundation for Research Science and Technology. We appreciate discussions with Leon Knopoff, Paul Davis, Rachel Abercrombie, Peter Koons, Rick Sibson, and Richard Norris. This is Institute of Geological and Nuclear Sciences Contribution Number 2391.

References

- Abercrombie, R. E. (1995). Earthquake source scaling relationships from -1 to $5 M_L$ using seismograms recorded at 2.5-km depth, *J. Geophys. Res.*, **100**, 24,015–24,036.
- Abercrombie, R. E., S. Bannister, A. Pancha, T. H. Webb, and J. J. Mori (2001). Determination of fault planes in a complex aftershock sequence using two-dimensional slip inversion, *Geophys. J. Int.*, **146**, 134–142.

- Allis, R. G. (1986). Mode of crustal shortening adjacent to the Alpine fault, New Zealand, *Tectonics* **5**, 15–32.
- Allis, R. G., and Y. Shi (1995). New insights to temperature and pressure beneath the central Southern Alps, New Zealand, *N. Z. J. Geol. Geophys.* **38**, 585–592.
- Anderson, O. L., and D. Isaak (1995). Elastic constants of mantle minerals at high temperature, in *Mineral Physics and Crystallography: A Handbook of Physical Constants*, T. J. Ahrens (Editor), AGU Reference Shelf, American Geophysical Union, Washington D.C., Vol. 2, 64–97.
- Anderson, H., D. Eberhart-Phillips, T. McEvilly, F. Wu, and R. Uhrhammer (1997). Southern Alps passive seismic experiment, Inst. of Geol. and Nuclear Sciences Sci. Rep. 97/21.
- Anderson, H., and T. Webb (1994). New Zealand seismicity patterns revealed by the upgraded National Seismograph Network, *N. Z. J. Geol. Geophys.* **37**, 477–493.
- Beaumont, C., P. J. J. Kamp, J. Hamilton, and P. Fullsack (1996). The continental collision zone: South Island, New Zealand: comparison of geodynamical models and observations, *J. Geophys. Res.* **101**, 3333–3359.
- Beavan, J., M. Moore, C. Pearson, M. Henderson, B. Parsons, S. Bourne, P. England, D. Walcott, G. Blick, D. Kirby, and K. Hodgkinson (1999). Crustal deformation during 1994–1998 due to oblique continental collision in the central Southern Alps, New Zealand, and implications for seismic potential of the Alpine fault, *J. Geophys. Res.* **104**, 25,233–25,255.
- Chen, W.-P., and P. Molnar (1983). Focal depths of intracontinental and intraplate earthquakes and their implications for the thermal and mechanical properties of the lithosphere, *J. Geophys. Res.* **88**, 4183–4214.
- Davey, F. J., T. Henyey, W. S. Holbrook, D. Okaya, T. A. Stern, A. Melhuish, S. Henrys, H. Anderson, D. Eberhart-Phillips, T. McEvilly, R. Uhrhammer, F. Wu, G. R. Jiracek, P. E. Wannamaker, G. Caldwell, and N. Christensen (1998). Preliminary results from a geophysical study across a modern, continent-continent collisional plate boundary; the Southern Alps, New Zealand *Tectonophysics* **288**, 221–235.
- Eberhart-Phillips, D., and S. Bannister (2002). Southern Alps, New Zealand, three-dimensional seismic velocity structure, *J. Geophys. Res.* (in press).
- Eberhart-Phillips, D., and M. Reyners (1997). Continental subduction and three-dimensional crustal structure: the northern South Island, New Zealand, *J. Geophys. Res.* **102**, 11,843–11,861.
- Eberhart-Phillips, D., and M. Reyners (2001). A complex, young subduction zone imaged by three-dimensional seismic velocity, Fiordland, New Zealand, *Geophys. J. Int.* **146**, 731–746.
- Gerbault, M., F. Davey, and S. Henrys (2002). Three-dimensional lateral crustal thickening in continental oblique collision: an example from the Southern Alps, New Zealand, *Geophys. J. Int.* (in press).
- Gomberg, J. S., K. M. Shedlock, and S. W. Roecker (1990). The effect of S-wave arrival times on the accuracy of hypocenter estimation, *Bull. Seism. Soc. Am.* **80**, 1605–1628.
- Gutenberg, B., and C. F. Richter (1941). Seismicity of the Earth, *Geol. Soc. Amer. Spec. Pap.* **34**, 1–141.
- Gutenberg, B., and C. F. Richter (1944). Frequency of earthquakes in California, *Bull. Seism. Soc. Am.* **34**, 185–188.
- Hadley, D., and H. Kanamori (1977). Seismic structure of the Transverse Ranges, California, *Geol. Soc. Am. Bull.* **88**, 1469–1478.
- Haines, A. J., I. M. Cahaem, and D. E. Ware (1979). Crustal seismicity near Lake Pukaki, South Island, *R. Soc. N. Z. Bull.* **18**, 87–94.
- Hearn, T. M., and R. W. Clayton (1986). Lateral velocity variations in Southern California. II. Results for the lower crust from Pn waves, *Bull. Seism. Soc. Am.* **76**, 511–520.
- Hirth, G., and J. Tullis (1994). The brittle-plastic transition in experimentally deformed quartz aggregates, *J. Geophys. Res.* **99**, 11,731–11,748.
- Houseman, G. A., E. A. Neil, and M. D. Kohler (2000). Lithospheric instability beneath the Transverse Ranges of California, *J. Geophys. Res.* **105**, 16,237–16,250.
- Humphreys, E. D., and R. W. Clayton (1990). Tomographic image of the Southern California mantle, *J. Geophys. Res.* **95**, 19,725–19,746.
- Kirby, S. H. (1980). Tectonic stresses in the lithosphere: constraints provided by the experimental deformation of rocks, *J. Geophys. Res.* **85**, 6353–6363.
- Kohler, M. D., and D. Eberhart-Phillips (2002). Three-dimensional lithospheric structure below the New Zealand Southern Alps, *J. Geophys. Res.* (in press).
- Leitner, B., D. Eberhart-Phillips, H. Anderson, and J. L. Nabelek (2001). A focused look at the Alpine fault, New Zealand: seismicity, focal mechanisms and stress observations, *J. Geophys. Res.* **106**, 2193–2220.
- Maggi, A., J. A. Jackson, K. Priestley, and C. Baker (2000). A re-assessment of focal depth distributions in southern Iran, the Tien Shan and northern India: do earthquakes really occur in the continental mantle? *Geophys. J. Int.* **143**, 629–661.
- Mori, J., Abercrombie, R. E., and H. Kanamori, H. (2000). Stress drops and radiated energies of aftershocks of the 1994 Northridge, California, earthquake, *J. Geophys. Res.* (submitted for publication).
- Norris, R. J., and A. F. Cooper (2000). Late Quaternary slip rates and slip partitioning on the Alpine Fault, New Zealand, *J. Struct. Geol.* **23**, 507–520.
- Norris, R. J., P. Koons, and A. F. Cooper (1990). The obliquely-convergent plate boundary in the South Island of New Zealand: implications for ancient collision zones, *J. Struct. Geol.* **12**, 715–725.
- Pysklywec, R. N., C. Beaumont, and P. Fullsack (2002). Lithospheric deformation during the early stages of continental collision: numerical experiments and comparison with South Island, New Zealand, *J. Geophys. Res.* (submitted for publication).
- Reilly, W. I., and C. M. Whiteford (1979). Gravity map of New Zealand, Bouguer and isostatic anomalies, South Island, Dep. of Sci. and Industrial Res. Wellington, scale 1:1,000,000.
- Reyners, M. (1987). Subcrustal earthquakes in the central South Island, New Zealand, and the root of the Southern Alps, *Geology* **15**, 1168–1171.
- Reyners, M. (1988). Reservoir induced seismicity at Lake Pukaki, New Zealand, *Geophys. J. Int.* **93**, 127–135.
- Richards-Dinger, K. B., and P. M. Shearer (1997). Estimating crustal thickness in Southern California by stacking PmP arrivals, *J. Geophys. Res.* **102**, 15,211–15,224.
- Richards-Dinger, K. B., and P. M. Shearer (2000). Earthquake locations in Southern California obtained using source-specific station terms, *J. Geophys. Res.* **105**, 10,939–10,960.
- Robinson, R., and T. Webb (1996). “Amprat” and Mechtool”: Programs for determining focal mechanism of local earthquakes, rep. 7, Inst. of Geol. and Nucl. Sci., Lower Hutt, New Zealand.
- Scholz, C. H. (1990). *The Mechanics of Earthquakes and Faulting*, Cambridge University Press, New York, 439 pp.
- Smith, E. C. G., T. A. Stern, and B. O’Brien (1995). A seismic velocity model for the central South Island, New Zealand, *N. Z. J. Geol. Geophys.* **38**, 565–571.
- Stern, T., P. Molnar, D. Okaya, and D. Eberhart-Phillips (2000). Teleseismic P wave delays and modes of shortening the mantle lithosphere beneath South Island, New Zealand, *J. Geophys. Res.* **105**, 21,615–21,631.
- Stern, T. A., P. E. Wannamaker, D. Eberhart-Phillips, D. Okaya, F. J. Davey, and S. I. P. W. Group (1997). Mountain building and active deformation studied in New Zealand, *EOS* **78**, 329, 335–336.
- Sutherland, R., F. Davey, and J. Beavan (2000). Plate boundary deformation in South Island, New Zealand, is related to inherited lithospheric structure, *Earth Planet. Sci. Lett.* **177**, 141–151.
- Turcotte, D. L., and G. Schubert (1982). *Geodynamics: Applications of Continuum Physics to Geological Problems*, Wiley & Sons, Inc., New York, 450 pp.

- Walcott, R. I. (1978). Present tectonics and Late Cenozoic evolution of New Zealand, *Geophys. J. R. Astr. Soc.* **52**, 137–164.
- Walcott, R. I. (1998). Modes of oblique compression: late Cenozoic tectonics of the South Island of New Zealand, *Rev. Geophys.* **36**, 1–26.
- Wellman, H. W. (1953). Data for the study of Recent and late Pleistocene faulting in the South Island of New Zealand, *N. Z. J. Sci. Technol.* **B34**, 270–288.
- Wilson, D., and D. Eberhart-Phillips (1998). Estimating crustal thickness in the central South Island, *Inst. Geol. & Nucl. Sci. Sci. Rep.* 98/27.
- Woodward, D. J. (1979). The crustal structure of the Southern Alps, New Zealand, as determined by gravity, in *The Origin of the Southern Alps*, R. I. Walcott and M. M. Cresswell (Editors), *Bull. R. Soc. N. Z.* **18**, 95–98.
- Department of Earth and Space Sciences
545 Charles E. Young Drive
Geology 3806
University of California, Los Angeles
Los Angeles, California 90095-1567
kohler@ess.ucla.edu
(M.D.K.)
- Institute of Geological and Nuclear Sciences
Private Bag 1930
Dunedin, New Zealand
D.Eberhart-Phillips@gns.cri.nz
(D.E.-P.)

Manuscript received 24 January 2002.